Article

Unraveling the Role of Stereo-electronic, Dynamical, and Environmental Effects in Tuning the Structure and Magnetic Properties of Glycine Radical in Aqueous Solution at Different pH Values

Giuseppe Brancato, Nadia Rega, and Vincenzo Barone

J. Am. Chem. Soc., **2007**, 129 (49), 15380-15390 • DOI: 10.1021/ja074910t

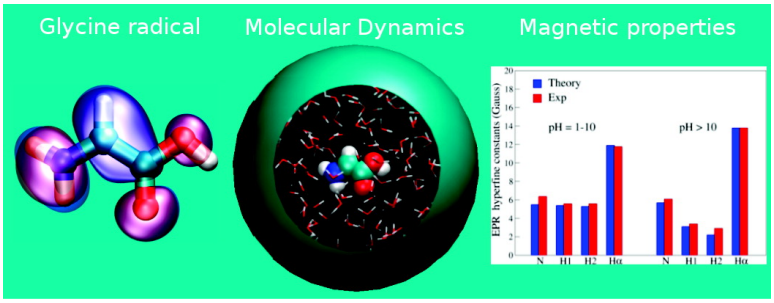

More About This Article

Additional resources and features associated with this article are available within the HTML version:

- Supporting Information
- Access to high resolution figures
- Links to articles and content related to this article
- Copyright permission to reproduce figures and/or text from this article

View the Full Text HTML

J|A|C|S
ARTICLES
Published on Web 11/16/2007

Unraveling the Role of Stereo-electronic, Dynamical, and Environmental Effects in Tuning the Structure and Magnetic Properties of Glycine Radical in Aqueous Solution at Different pH Values

Giuseppe Brancato, Nadia Rega, and Vincenzo Barone*

Contribution from the Chemistry Department Paolo Corradini, University Federico II, Complesso Universitario Monte S. Angelo, via Cintia, I-80126 Napoli, Italy

Received July 4, 2007; E-mail: baronev@unina.it

Abstract: A recently developed extended Lagrangian model employing localized basis functions and nonperiodic boundary conditions (GLOB/ADMP) was applied to the radicals issuing from the homolytic breaking of the $C^{\alpha}-H^{\alpha}$ bond of glycine in aqueous solution at different pH values. Although the modifications of the structure and the magnetic properties of these species induced by the solvent are qualitatively reproduced by a static discrete-continuum model, magnetic parameters are further tuned by short-time dynamical effects (solute vibrations and solvent librations). The results delivered by GLOB/ADMP simulations for both hyperfine tensors and **g**-tensors are in remarkable agreement with their experimental counterparts, allowing a reliable disentanglement of the overall observables into well-defined contributions. The dominant role of out-of-plane vibrations in determining hyperfine splittings is confirmed and quantified, together with the remarkable sensitivity of the gyromagnetic tensor to bond lengths and valence angles defining the $NC^{\alpha}C'$ moiety. Together with their specific interest for the title radical, our results suggest some interesting trends for other biologically significant radicals and point out the need of extending magneto-structural relationships to dynamical aspects.

1. Introduction

The role of photoreactions in solution in a number of processes of biological and/or technological relevance is widely acknowledged,[1−6] but several aspects are still not fully characterized, and a deeper understanding of these would strongly benefit from interplay between fast experimental methods and reliable quantum mechanical computations. Here, we will be concerned with aliphatic radicals issuing from elimination reactions involving amino acids and their derivatives, which are usually α-carbon-centered radicals. Already the simplest amino acid, glycine, and its derivatives show a number of unexpected features (e.g., preference for neutral or zwitterionic structure in different condensed phases, anomalously low hydrogen hyperfine coupling in aqueous solution), which have stimulated a large number of experimental[7−12] and theoretical[13−22] studies. Although a number of features have been analyzed, a better understanding of general trends requires, in our opinion, integrated strategies in which well-defined models are investigated by both experimental and theoretical approaches.[23,24] As mentioned above, interpretation of experimental results is not without ambiguities, either because of the role of different environmental effects or because the relationship between spectroscopic and structural/dynamics characteristics is only indirect.[25] Here, theoretical approaches come into play, provided that they are able to couple reliability and feasibility for large systems.[26] In this connection, models rooted into the density

(1) Stuble, J. A. *Annu. Rev. Biochem.* **1989**, *58*, 257.
(2) Baldwin, J. E.; Bradley, M. *Chem. Rev.* **1990**, *90*, 1079.
(3) Von Sonntag, C. *The Chemical Basis of Radiation biology*; Taylor and Francis: New York 1987.
(4) Stadman, E. R. *Annu. Rev. Biochem.* **1993**, *62*, 797.
(5) Easton, C. J. *Chem. Rev.* **1997**, *97*, 53.
(6) Xerri, B.; Morell, C.; Grand, A.; Cadet, J.; Cimino, P.; Barone, V. *Org. Biomol. Chem.* **2006**, *4*, 3986.
(7) Ghosh, D. H.; Wiffen, D. H. *J. Chem. Soc.* **1960**, 1869.
(8) Paul, v. H.; Fischer, H. *Helv. Chim. Acta* **1971**, *54*, 485.
(9) Neta, P.; Fessenden, R. W. *J. Phys. Chem.* **1971**, *75*, 738.
(10) Armstrong, D. A.; Rauk, A.; Yu, D. *J. Chem. Soc., Perkin Trans 2* **1995**, 553.
(11) Brustolon, M.; Chis, V.; Maniero, A. L.; Brunel, L.-C. *J. Phys. Chem. A* **1997**, *101*, 4887.
(12) Sanderud, A.; Sagstuen, E. *J. Phys. Chem. B* **1998**, *102*, 9353.
(13) (a) Yu, D.; Rauk, A.; Armstrong, D. A. *J. Am. Chem. Soc.* **1995**, *117*, 1789. (b) Yu, D.; Rauk, A.; Armstrong, D. A. *J. Am. Chem. Soc.* **1997**, *119*, 208.
(14) Barone, V.; Adamo, C.; Grand, A.; Brunel, Y.; Fontecave, M.; Subra, R. *J. Am. Chem. Soc.* **1995**, *117*, 1083.
(15) Barone, V.; Adamo, C.; Grand, A.; Subra, R. *Chem. Phys. Lett.* **1995**, *242*, 35.
(16) (a) Barone, V.; Adamo, C.; Grand, A.; Jolibois, F.; Brunel, Y.; Subra, R. *J. Am. Chem. Soc.* **1995**, *117*, 12618. (b) Barone, V.; Capecchi, G.; Brunel, Y.; Dheu Andries, M. L.; Subra, R. *J. Comput. Chem.* **1997**, *14*, 1720.
(17) Rega, N.; Cossi, M.; Barone V. *J. Am. Chem. Soc.* **1997**, *119*, 12962.
(18) Rega, N.; Cossi, M.; Barone, V. *J. Am. Chem. Soc.* **1998**, *120*, 5723.
(19) Pawels, E.; Van Speybroeck, V.; Waroquier, M. *J. Phys. Chem. B* **2004**, *108*, 11321.
(20) Ciofini, I.; Adamo, C.; Barone, V. *J. Chem. Phys.* **2004**, *121*, 6710.
(21) Kaprzac, S.; Reviakine, R.; Kaupp, M. *J. Phys. Chem. B* **2007**, *111*, 811.
(22) Kaprzac, S.; Reviakine, R.; Kaupp, M. *J. Phys. Chem. B* **2007**, *111*, 820.
(23) Barone, V.; Brustolon, M.; Cimino, P.; Polimeno, A.; Zerbetto, M.; Zoleo, A. *J. Am. Chem. Soc.* **2006**, *128*, 15865.
(24) (a) Zerbetto, M.; Carlotto, S.; Polimeno, A.; Corvaja, C.; Franco, L.; Toniolo, C.; Formaggio, F.; Barone, V.; Cimino, P. *J. Phys. Chem. B* **2007**, *111*, 2868. (b) S. Carlotto, S.; Cimino, P.; Zerbetto, M.; Franco, L.; Corvaja, C.; Crisma, M.; Formaggio, F.; Toniolo, C.; Polimeno, A.; Barone, V. *J. Am. Chem. Soc.* **2007**, *129*, 11248.
(25) Polimeno, A.; Barone, V. *Phys. Chem. Chem. Phys.* **2006**, *8*, 4609.
(26) Improta, R.; Barone, V. *Chem. Rev.* **2004**, *104*, 1231.

10.1021/ja074910t CCC: $37.00

functional theory (DFT) are today the methods of choice for the description of structural and spectroscopic characteristics of large, flexible radicals.[27,28] At the same time, approaches in which the solvent degrees of freedom are accounted for in an average way in terms of a reaction field[29,30] have proven particularly effective, leading in a number of cases to substantial improvement in energies, geometries, and spectroscopic parameters computed in a variety of solvent media.[31,32] However, in some instances implicit solvent models may also display limitations, e.g., in situations where highly specific interactions, like hydrogen bonds, come into play.[33] Supermolecule approaches can then provide a straightforward route to describe the influence of solvent molecules on localized phenomena, including spectroscopic parameters: again, implicit models can be brought into play to account for the "bulk" solvent, and thus to reduce the number of solvent molecules that need to be described explicitly.[34] The same explicit/implicit model is also attractive for the computation of averaging effects brought about by dynamics when a spectroscopic transition is fast with respect to the time scale of a dynamical phenomenon. Since in these cases the measured parameters represent weighted averages over the configurations with significant populations, if a representative molecular dynamics simulation has been generated, the statistical distribution of the parameter values in the system can be reproduced by extracting from the trajectory a sufficient number of representative frames and repeating a computation on each one of them: thus, averaging of the computed values provides an estimate of the experimental measurement.[35,36] Simulations employing energies and gradients computed by quantum mechanical (QM) methods are starting to provide classical trajectories which are long enough to allow reliable averaging of spectroscopic parameters.[37,38] In this framework, we have recently developed a general model, hereafter referred to as GLOB (general liquid optimized boundary), enforcing

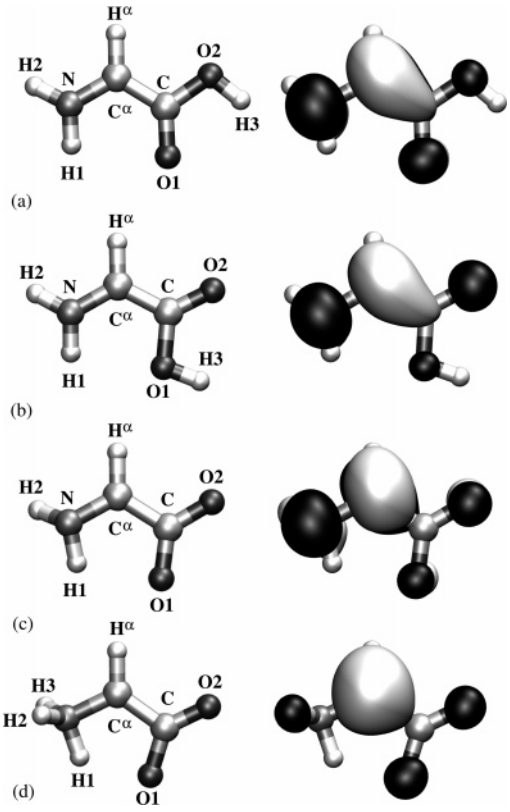

Figure 1. Gas-phase structures, atom labels, and SOMOs of (a) $GlyR^{cis}$, (b) $GlyR^{trans}$, (c) $GlyR^{-}$, and (d) $GlyR^{zw}$. A threshold value of 0.05 has been adopted in the plots of the molecular orbitals.

nonperiodic boundary conditions, which are more suitable for *ab initio* dynamic simulations employing localized basis functions.[39,40] Thus, we are able to take into account at the same time solvent librations and solute vibrations, both of which can lead to non-negligible averaging effects of spectroscopic parameters.[41] In the absence of significant solute−solvent electron or spin transfer, an integrated approach in which a full QM description of the solute is coupled to a molecular mechanics (MM) modeling of a few water shells embedded in the GLOB boundary represents the most effective and reliable solution due to the existence of very reliable force fields for water that can reproduce satisfactory bulk behavior, providing results in good agreement with more demanding full QM simulations.[42] Thus, all short-time dynamical effects in solution should be well accounted for by reliable QM/MM/implicit solvent approaches based on extended Lagrangian dynamics.

From a complementary point of view, dynamical processes that occur on a time scale comparable to that of the spectroscopic transition have a direct influence on signal line shape, and their description in terms of the stochastic Liouville equation (SLE) is providing remarkably faithful reproductions of complex high-

(27) (a) Barone, V.; Adamo, C.; Russo, N. *Chem. Phys. Lett.* **1993**, *212*, 5. (b) Barone, V. *J. Chem. Phys.* **1994**, *101*, 6834. (c) Barone, V. *J. Chem. Phys.* **1994**, *101*, 10666. (d) Barone, V.; Adamo, C. *Chem. Phys. Lett.* **1994**, *224*, 432. (e) Barone, V. *Theor. Chem. Acc.* **1995**, *91*, 113. (f) Barone, V. In *Advances in Density Functional Theory*; Chong, D. P., Ed.; World Scientific Publ. Co.: Singapore, 1995; Part I, p 287. (g) Engels, B.; Eriksson, L. A.; Lunell, S. *Advances in Quantum Chemistry*; Academic Press: San Diego, CA, 1996; Vol. 27, p 297.
(28) (e) Mattar, S. M. *Chem. Phys. Lett.* **1998**, *287*, 608. (b) Mattar, S. M.; Stephens, A. D. *Chem. Phys. Lett.* **2000**, *319*, 601. (c) Arbuznikov, A. V.; Kaupp, M.; Malkin, V. G.; Reviakine, R.; Malkina, O. L. *Phys. Chem. Chem. Phys.* **2002**, *4*, 5467. (d) Mattar, S. M. *J. Phys. Chem. B* **2004**, *108*, 9449. (e) Sinnecker, S.; Reijerse, E.; Neese, F.; Lubitz, W. *J. Am. Chem. Soc.* **2004**, *126*, 3280. (f) Neugerbauer, J.; Louwerse, M. J.; Belanzoni, P.; Wesolowski, T. A.; Baerends, E. J. *J. Chem. Phys.* **2005**, *109*, 445. (g) Schoneborn, J. C.; Neese, F.; Thiel, W. *J. Am. Chem. Soc.* **2005**, *127*, 5840. (h) Astashkin, A. V.; Neese, F.; Raitsimiring, A. M.; Cooney, J. J. A.; Bultman, E.; Enemark, J. H.; Neese, F. J. *J. Am. Chem. Soc.* **2005**, *127*, 16713. (i) Mattar, S. M. *J. Phys. Chem. A* **2007**, *111*, 251.
(29) Cramer, C. J.; Truhlar, D. G. *Chem. Rev.* **1999**, *99*, 2161.
(30) Tomasi, J.; Mennucci, B.; Cammi, R. *Chem. Rev.* **2005**, *105*, 2999.
(31) (a) Mennucci, B.; Toniolo, A.; Tomasi, J. *J. Am. Chem. Soc.* **2000**, *122*, 10621. (b) Barone, V.; Cimino, P.; Crescenzi, O.; Pavone, M. *Theochem* **2007**, *811*, 323.
(32) (a) Barone, V. *Chem. Phys. Lett.* **1996**, *262*, 201. (b) Rega, N.; Cossi, M.; Barone, V. *J. Chem. Phys.* **1996**, *105*, 11060. (c) di Matteo, A.; Adamo, C.; Cossi, M.; Rey, P.; Barone, V. *Chem. Phys. Lett.* **1999**, *310*, 159.
(33) Langella, E.; Improta, R.; Barone, V. *J. Am. Chem. Soc.* **2002**, *124*, 11531.
(34) (a) Adamo, C.; di Matteo, A.; Rey, P.; Barone, V. *J. Phys. Chem. A* **1999**, *103*, 3481. (b) Tedeschi, A. M.; D'Errico, G.; Busi, E.; Basosi, R.; Barone, V. *Phys. Chem. Chem. Phys.* **2002**, *4*, 2180. (c) Cimino, P.; Pavone, M.; Barone, V. *Chem. Phys. Lett.* **2005**, *409*, 106.
(35) Georg, H. C.; Coutinho, K.; Canuto, S. *J. Chem. Phys.* **2005**, *123*, 124307.
(36) Pavone, M.; Brancato, G.; Morelli, G.; Barone, V. *Chem. Phys. Chem* **2006**, *7*, 148.
(37) (a) Nillson, J. A.; Eriksson, L. A.; Laaksonen, A. *Mol. Phys.* **2001**, *99*, 247. (b) Nonella, M.; Mathias, G.; Tavan, P. *J. Phys. Chem. A* **2003**, *107*, 8638. (c) Asher, J. R.; Doltsinis, N. L.; Kaupp, M. J. *Magn. Reson. Chem.* **2005**, *43*, S237.
(38) (a) Pavone, M.; Benzi, C.; De Angelis, F.; Barone, V. *Chem. Phys. Lett.* **2004**, *395*, 120. (b) Pavone, M.; Cimino, P.; De Angelis, F.; Barone, V. *J. Am. Chem. Soc.* **2006**, *128*, 4338. (c) Pavone, M.; Sillampa, A.; Cimino, P.; Crescenzi, O.; Barone, V. *J. Phys. Chem. B* **2006**, *110*, 16189.
(39) (a) Rega, N.; Brancato, G.; Barone, V. *Chem. Phys. Lett.* **2006**, *422*, 367. (b) Brancato, G.; Rega, N.; Barone, V. *J. Chem. Phys.* **2006**, *124*, 214505. (c) Brancato, G.; Rega, N.; Barone, V. *J. Chem. Phys.* **2006**, *125*, 164515.
(40) Brancato, G.; Barone, V.; Rega, N. *Theor. Chem. Acc.* **2007**, *117*, 1001.
(41) (a) Barone, V.; Subra, R. *J. Chem. Phys.* **1996**, *104*, 2630. (b) Jolibois, F.; Cadet, J.; Grand, A.; Subra, R.; Rega, N. *J. Am. Chem. Soc.* **1998**, *120*, 1864. (c) Barone, V. *J. Chem. Phys.* **2005**, *122*, 014108. (d) Barone, V.; Carbonniere, P.; Pouchan, C. *J. Chem. Phys.* **2005**, *122*, 224308.
(42) Todorova, T.; Seitsonen, A.; Hutter, J.; Kuo, I.-F.; Mundy, C. *J. Phys. Chem. B* **2006**, *110*, 3685.

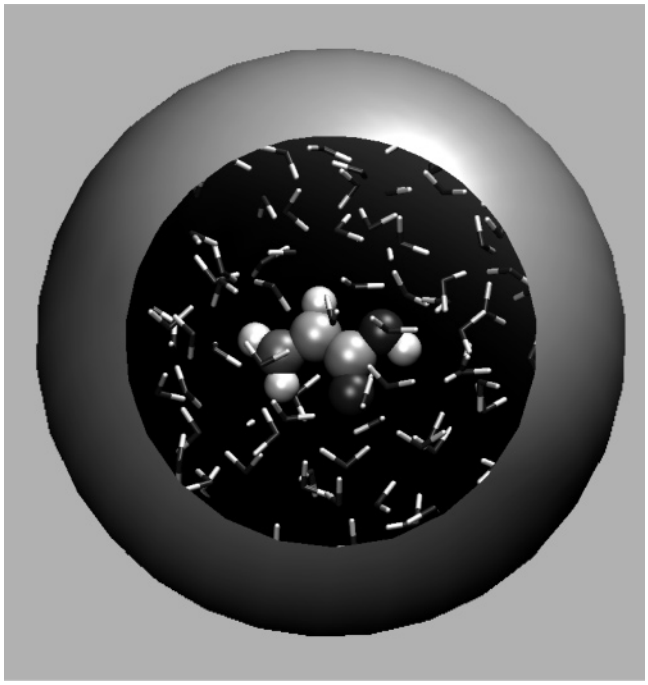

Figure 2. Sketch of the molecular system (glycine radical + water) simulated using the GLOB/ADMP model.

field electron paramagnetic resonance (EPR) spectra.[43] However, the computation of reliable magnetic tensors averaged over short-time motions (solute vibrations and solvent librations), which is the specific topic of the present contribution, represents a mandatory and nontrivial starting point for the replacement of spectra fitting by *a priori* spectra forecasting by integrated QM/SLE approaches.[23−25] In the following we will show, for the specific case of glycine radical at different pH values, that the route is being paved toward this goal even for flexible molecules in aqueous solution.

2. Computational Details

2.1. Molecular Dynamics Simulations. Different pH conditions and isomerism of the glycine radical in aqueous solution were investigated by considering, together with the anionic form (NH_2CHCOO^-, hereafter $GlyR^-$), three neutral species, either zwitterionic ($NH_3^+CHCOO^-$, hereafter $GlyR^{zw}$) or not ($NH_2CHCOOH$, hereafter $GlyR^{cis}$ and $GlyR^{trans}$) (see Figure 1). Four GLOB/ADMP (atom-centered density matrix propagation) simulations of such species in aqueous solution at room temperature (300 K) have been carried out for about 50 ps, including 4 ps of equilibration. This model (see Figure 2)[39,40] is particularly well-suited for treating solute−solvent systems of variable size and at different levels of theory, from purely classical force field based methods (usually referred to as MM approaches) to more sophisticated hybrid QM/MM and full QM methodologies. In particular, the solute, representing the quantum "core" in the QM/MM partitioning scheme, has been treated at the DFT level with the well-trusted B3LYP functional,[44] whereas the remaining solvent (water) molecules are modeled at lower MM level, according to the TIP3P model.[45] In all simulations we have used the recently developed N06 basis set,[46] which provides comparable results in terms of molecular geometries and electric dipole moments to more extended basis sets (*vide infra*) and reduces significantly the basis set superposition error (BSSE).

Table 1. Intermolecular Lennard-Jones Parameters of the Glycine Radical

	$GlyR^{cis/trans}$		$GlyR^{zw}$		$GlyR^-$	
	σ	ϵ	σ	ϵ	σ	ϵ
N	3.86	0.13	3.47	0.13	3.86	0.13
H1	1.06	0.03	1.06	0.03	1.06	0.03
H2	1.06	0.03	1.06	0.03	1.06	0.03
C^α	4.02	0.06	4.02	0.06	4.02	0.06
H^α	2.22	0.03	2.22	0.03	2.22	0.03
C	4.02	0.06	4.02	0.06	4.02	0.06
O1	3.33	0.19	3.12	0.19	3.12	0.19
O2	3.33	0.19	3.12	0.19	3.12	0.19
H3	1.06	0.03	1.06	0.03		

Preliminary full QM calculations on various glycine radical/water clusters have shown a negligible charge and spin transfer between the radical and water molecules, supporting the use of the present effective approach. Interactions between the QM and MM regions consist, as usual, of both electrostatic and van der Waals interactions and are modeled according to the B3LYP/AMBER potential parametrized by Freindorf et al.[47] Note that, in the case of the anionic and zwitterionic form of the glycine radical, the Lennard-Jones parameters of the nitrogen and oxygen atoms were slightly modified to better match geometrical configurations of glycine radical/water clusters (see Table 1).

Moreover, both QM and MM interactions with bulk solvent (continuum) were taken into account by a mean field approach including an exact treatment of the electrostatic "reaction field" and an effective representation of short-range dispersion−repulsion interactions derived so as to minimize edge effects on the solvent density and average energy.[39,40] During the dynamics, the electron density matrix has been propagated "on the fly", along with the nuclei, according to the ADMP method.[48] The core and valence orbitals were weighted differently during the dynamics, with $\mu_{valence} = 0.1$ amu bohr$^2 \approx 180$ au for the valence electrons and μ_{core} obtained according to the tensorial fictitious mass scheme described in ref 48. In all cases considered ($GlyR^{cis}$, $GlyR^{trans}$, $GlyR^-$, and $GlyR^{zw}$), the solute was embedded with 134 TIP3P water molecules into a spherical cavity with a radius of 10.0 Å, whereas the electrostatic reaction field was evaluated with respect to a dielectric continuum on a sphere with radius 11.8 Å, according to the conductor-like version of the PCM (CPCM).[49] The center of mass of the glycine radical was constrained at the center of the cavity, and the mean-field nonelectrostatic contribution employed was parametrized for a TIP3P water system of size corresponding to the system considered in this work.[39,40] A constant thermal energy (300 K) has been enforced by scaling nuclear velocities every 2500 steps, with a time step of 0.2 fs.

2.2. Quantum Mechanical Calculations of EPR Parameters. The EPR parameters of glycine radical at different pH values in aqueous solution have been computed from the MD trajectories and compared with available experimental data recorded in solution[7−10] and in the solid state.[11,12] Statistical averages have been performed on *a posteriori* quantum mechanical calculations of a large number (about 500) of molecular configurations sampled during the MD simulations. Such

(43) (a) Schneider, D. J.; Freed, J. H. *Adv. Chem. Phys.* **1989**, *73*, 487. (b) Polimeno, A.; Freed, J. H. *Adv. Chem. Phys.* **1992**, *83*, 89.
(44) (a) Becke, A. *J. Chem. Phys.* **1993**, *98*, 5648. (b) Stephens, P. J.; Devlin, F. J.; Chabalowski, C. F.; Frisch, M. J. *J. Phys. Chem.* **1994**, *98*, 11623.
(45) Jorgensen, W. L.; Chandrasekhar, J.; Madura, J. D.; Impey, R. W.; Klein, M. L. *J. Chem. Phys.* **1983**, *79*, 926.
(46) The N06 basis set was obtained by adding to the Pople 6-31G basis set single sets of optimized core-valence s (on all atoms except H), diffuse s (on H), diffuse p (on all atoms except H), polarization (on all atoms), and diffuse d (on O atoms) gaussian functions.
(47) Freindof, M.; Shao, Y.; Furlani, T. R.; Kong, J. *J. Comput. Chem.* **2005**, *26*, 1270.
(48) (a) Schlegel, H. B.; Millam, J. M.; Iyengar, S. S.; Voth, G. A.; Daniels, A. D.; Scuseria, G. E.; Frisch, M. J. *J. Chem. Phys.* **2001**, *114*, 9758. (b) Iyengar, S. S.; Schlegel, H. B.; Millam, J. M.; Voth, G. A.; Scuseria, G. E.; Frisch, M. J. *J. Chem. Phys.* **2001**, *115*, 10291. (c) Schlegel, H. B.; Iyengar, S. S.; Li, X.; Millam, J. M.; Voth, G. A.; Scuseria, G. E.; Frisch, M. J. *J. Chem. Phys.* **2002**, *117*, 8694. (d) Rega, N.; Iyengar, S. S.; Voth, G. A.; Schlegel, H. B.; Vreven, T.; Frisch, M. J. *J. Phys. Chem. B* **2004**, *108*, 4210.
(49) (a) Barone, V.; Cossi, M. *J. Phys. Chem. A* **1998**, *102*, 1995. (b) Cossi, M.; Scalmani, G.; Rega, N.; Barone, V. *J. Comput. Chem.* **2003**, *24*, 669.

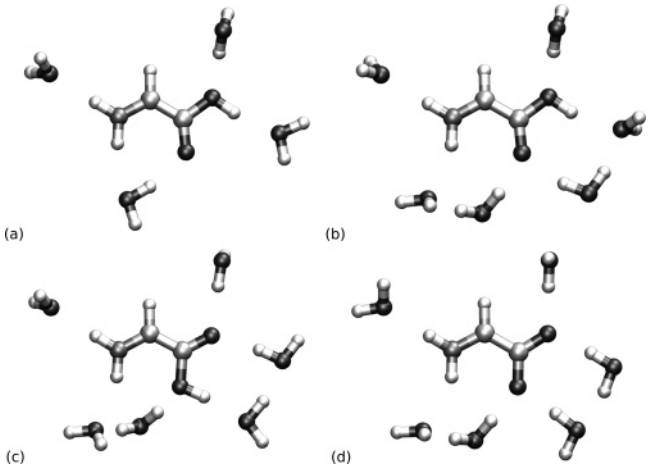

Figure 3. Optimized glycine radical−water clusters: GlyR^{cis} with (a) four and (b) six water molecules, (c) GlyR^{trans} with six water molecules, and (d) GlyR^- with six water molecules. See text for further details.

spectroscopic calculations were carried out on the basis of the same explicit molecular system and QM/MM partition (glycine radical, B3LYP; 134 water molecules, TIP3P) used in the ADMP simulations, the only difference being the use of the purposely tailored EPR-III basis set.[50]

The hyperfine coupling tensor ($\mathbf{A}_X$), which describes the interaction between the electronic spin density and the nuclear magnetic momentum of nucleus X, can be split into three terms: $\mathbf{A}_X = a_X\mathbf{1}_3 + \mathbf{T}_X + \Lambda_X$, where $\mathbf{1}_3$ is the 3×3 unit matrix. The first term (a_X), usually referred to as Fermi contact interaction, is an isotropic contribution and is related to the spin density at the corresponding nucleus X. The second contribution ($\mathbf{T}_X$) is anisotropic and can be derived from the classical expression of interacting dipoles. The last term, Λ_X, is due to second-order spin−orbit coupling and can be determined by methods similar to those described in the following for the **g**-tensor. In the present case, because of the strong localization of spin density on first-row atoms and of their small spin−orbit coupling constants, its contribution can be safely neglected and will not be discussed in the following. Because both a_X and $\mathbf{T}_X$ are ruled by one-electron operators, their evaluation is, in principle, quite straightforward. However, hyperfine coupling constants have been among the most challenging quantities for conventional QM approaches for two main reasons.[26,27] On one hand, conventional Gaussian basis sets are ill adapted to describe nuclear cusps; on the other hand, the overall result derives from the difference between large quantities of opposite sign. However, the past few years have shown that coupling of some hybrid functionals (here B3LYP) to purposely tailored basis sets (here EPR-III) performs a remarkable job for both isotropic and dipolar terms.

The **g**-tensor can be written as follows: $\mathbf{g} = g_e\mathbf{1}_3 + \Delta\mathbf{g}_{RM} + \Delta\mathbf{g}_G + \Delta\mathbf{g}_{OZ/SOC}$, where g_e is the free-electron value ($g_e = 2.0023193$). Computation of the relativistic mass (RM) and gauge (G) corrections is quite straightforward because they are first-order contributions.[20] The last term arises from the coupling of the orbital Zeeman (OZ) and the spin−orbit coupling (SOC) operator. The OZ contribution is computed using the gauge-including atomic orbital (GIAO) approach,[20,51] whereas the two-electron SOC operator is approximated by a one-electron operator involving adjusted effective nuclear charges.[52] Once again, the B3LYP functional and the EPR-III basis set provide reliable results.[20−22] Upon complete averaging by rotational motions, only the isotropic parts of the $\mathbf{A}_N$ and **g**-tensors survive, which are given by $a_N = {}^1/_3\,\mathrm{Tr}(\mathbf{A}_N)$ and $g_{iso} = {}^1/_3\,\mathrm{Tr}(\mathbf{g})$. The isotropic part of the hyperfine tensor is usually referred to as the hyperfine coupling constant (hcc) and will be given in the following in Gauss (1 G = 0.1 mT). The isotropic part of the **g**-tensor is given in the following in terms of shift from the free electron value, $\Delta g_{iso} = g_{iso} - g_e$, and is expressed in parts per million (ppm).

For comparison, we have also carried out spectroscopic calculations on the isolated glycine radical at geometric configurations previously obtained from QM geometry optimizations, possibly including solvent effects in an effective way by means of the CPCM. It is worth noting that test calculations on different glycine radical/water clusters have shown no significant deviations of the EPR parameters considered in the present work between the full QM and mixed QM/MM approaches. All the simulations and quantum mechanical calculations have been performed with a locally modified version of the Gaussian package.[53]

3. Results and Discussion

Several studies on the structures and stabilities of C-centered glycine radicals[9,10,13,17,18] have shown that cationic species never predominate in aqueous solution and that, contrary to the parent molecule, at not too basic pH the neutral form ($NH_2CHCOOH$) is more stable than its zwitterionic counterpart ($NH_3^+CHCOO^-$). Above pH = 10, the anionic form (NH_2CHCOO^-) starts to prevail. We have thus analyzed both anionic and neutral forms, taking into account that, in the latter case, cis (GlyR^{cis}) and trans (GlyR^{trans}) placements of the oxidryl moiety with respect to the $C^\alpha-H^\alpha$ bond are not equivalent and are nearly isoenergetic. Although we have performed a GLOB/ADMP simulation also for the zwitterionic form, it will be not discussed in detail due to the negligible amount of this species in aqueous solution (*vide infra*).

3.1. Optimized Structures. The gas-phase structures of GlyR^{cis}, GlyR^{trans}, and GlyR^- have been studied at DFT and post-Hartree−Fock (second-order perturbation theory, MP2, and coupled clusters including single, double, and perturbative treatment of triple excitations, CCSD(T)) levels of theory in order to validate the quantum mechanical model employed in the molecular dynamics simulations (B3LYP/N06). Also, we have compared the intramolecular changes due to solvent effects by carrying out QM calculations on small glycine radical/water clusters and using the CPCM. In all cases, the most stable structure is nearly planar due to the delocalization effect of the unpaired electron, with the only exception being the aminic hydrogens. In Figure 1, the gas-phase optimized structures and atom labels of GlyR^{cis}, GlyR^{trans}, GlyR^-, and GlyR^{zw} are depicted, along with the corresponding singly occupied molecular orbitals (SOMOs), as obtained at the B3LYP/EPR-III level. A similar delocalized character is shown by the SOMOs, which are centered on the C^α atom but extend to both terminal groups of glycine. Only in the case of GlyR^{zw}, the electronic delocalization of the SOMO is hindered due to the different hybridization of the nitrogen atom. In Table 2, the gas-phase geometrical parameters and dipole moment of the optimized structure of GlyR^{cis} are reported. Some selected parameters of GlyR^{cis} involving heavy atoms ($N-C^\alpha$, $C^\alpha-C$, C=O1, and C−O2 bond lengths and the $N-C^\alpha-C$ angle) have been optimized at the CCSD(T) level, freezing the other structural parameters at their values optimized at the MP2/aug-cc-pVTZ level. In particular, we have made the following basis set extrapolation for each of the previous parameters, λ: λ(CCSD(T)/aug-cc-pVTZ) = λ-

(50) (a) Barone, V. *J. Phys. Chem.* **1995**, *91*, 113. (b) Rega, N.; Cossi, M.; Barone, V. *J. Chem. Phys.* **1996**, *105*, 11060.
(51) (a) Ditchfield, R. *Mol. Phys.* **1974**, *27*, 789. (b) Cheesman, J. R.; Trucks, G. W.; Keith, T. A.; Frisch, M. J. *J. Chem. Phys.* **1998**, *104*, 5497.
(52) Koseki, S.; Schmidt, M. W.; Gordon, M. S. *J. Phys. Chem.* **1992**, *96*, 10768.
(53) Frisch, M. J.; et al. *Gaussian03*, Revision C.02; Gaussian, Inc.: Wallingford CT, 2004.

Table 2. Gas-Phase Geometrical Parameters and Dipole Moment of $GlyR^{cis}$ Issuing from Quantum Mechanical Optimizations at Different Levels of Theory

	B3LYP[a]	B3LYP[b]	MP2[b]	CCSD(T)[b]
N—H1	1.013	1.008	1.009	
N—H2	1.008	1.002	1.002	
N—C^{α}	1.358	1.354	1.350	1.359
C^{α}—H^{α}	1.082	1.077	1.075	
C^{α}—C	1.429	1.426	1.430	1.433
C═O1	1.228	1.226	1.227	1.227
C—O2	1.367	1.367	1.359	1.364
O2—H3	0.970	0.967	0.969	
H1—N—H2	117.75	118.84	119.37	
N—C^{α}—C	118.21	118.09	116.37	116.82
O1—C—O2	122.30	122.27	122.76	
H1NC^{α}C	−9.51	−6.26	−6.70	
H2NC^{α}C	−165.03	−170.03	−170.07	
N$H^{\alpha}CC^{\alpha}$	1.57	0.96	1.17	
C^{α}CO2H3	−179.57	−179.74	−179.72	
μ	2.79	2.85	2.82	

[a] N06. [b] aug-cc-pVTZ.

(CCSD(T)/cc-pVTZ) + λ(MP2/aug-cc-pVTZ) − λ(MP2/cc-pVTZ). Overall, results obtained at the B3LYP level are in good agreement with computationally expensive post-Hartree Fock methods, with maximum deviations for bond lengths and valence angles of the order of 10^{-3} angstroms and a few degrees, respectively. Further, extrapolation of CCSD(T) results at the aug-cc-pVTZ level seems to improve the agreement with B3LYP. B3LYP/N06 results are very similar to their B3LYP/aug-cc-pVTZ counterparts at a significantly lower computational cost (the numbers of basis functions are N06, 125; aug-cc-pVTZ, 322). Only the dihedral angles of the NH_2 moiety are slightly larger, but it is worth noting that, in terms of the potential energy, such a discrepancy is lower than 0.1 kcal/mol. The computed electric dipole moment, which rules intermolecular interactions in polar solvents, does not change when going from B3LYP to MP2 models or from N06 to aug-cc-pVTZ basis sets. In Table 3, the structure and dipole moment of $GlyR^{cis}$ in solution are reported. Again, we observe a fairly good agreement between the structural parameters obtained at B3LYP/N06, B3LYP/aug-cc-pVTZ, and MP2/aug-cc-pVTZ levels using the CPCM. The MP2 model provides similar dipole moment and solvent shifts with respect to B3LYP. Specifically, inclusion of environmental effects induces a shortening of the N—C^{α} and C^{α}—C bonds, a lengthening of the carbonyl C═O1 bond, and an approximately planar configuration of the NH_2 group. To better model the specific hydrogen-bonding interactions occurring in aqueous solution, we have also considered two different $GlyR^{cis}$/water clusters with four and six water molecules, respectively (see Figure 3), including solvent bulk effects by means of the CPCM. For consistency with our simulation protocol, the water molecules are treated as classical particles according to the QM/MM scheme described in the Computational Details section. Results show a quite similar trend of the $GlyR^{cis}$ intramolecular rearrangements, with small differences in the bond angles due to the different water solvation cages.

We have next computed the minimum energy structures for $GlyR^{trans}$ and $GlyR^{-}$ in the gas-phase and in aqueous solution, in the latter case using the CPCM or including a few explicit water molecules plus the CPCM, as shown in Tables 4 and 5. The results confirm the general agreement between B3LYP and MP2 approaches and a qualitatively similar rearrangement of the molecule as a result of the interactions with the solvent. Additionally, the introduction of explicit water molecules hydrogen-bonded directly with glycine radical (see Figure 3) has the general result of enhancing the solvent effects on the radical geometry. Binding energies between 5 and 9 kcal/mol are computed for the interactions between water molecules and the neutral radical, which are comparable to the water−water interaction (5 kcal/mol). Of course, much larger binding energies (up to 16 kcal/mol) are obtained for the water molecules interacting with the carboxylate moiety of $GlyR^{-}$.

3.2. Simulations in Aqueous Solution. Three extended QM/MM simulations of $GlyR^{cis}$, $GlyR^{trans}$, and $GlyR^{-}$ in aqueous solution have been performed at room temperature (300 K), according to the GLOB/ADMP scheme described in the Computational Details section. The average structures of the solutes are reported in the last columns of Tables 2−4. The main structural changes around the formal radical center (C^{α}) in going from gas phase to aqueous solution involve the N—C^{α}, C^{α}—C, and C^{α}—H^{α} bonds, where the latter is lengthened [$\Delta(C^{\alpha}-H^{\alpha}) = +0.004$ Å] in GlyR (both cis and trans conformers) but not in $GlyR^{-}$, whereas the former are shortened in all cases [$GlyR^{cis}$, $\Delta(C^{\alpha}-C) = -0.003$ Å, $\Delta(N-C^{\alpha}) = -0.005$ Å; $GlyR^{trans}$, $\Delta(C^{\alpha}-C) = -0.002$ Å, $\Delta(N-C^{\alpha}) = -0.007$ Å; $GlyR^{-}$, $\Delta(C^{\alpha}-C) = -0.038$ Å, $\Delta(N-C^{\alpha}) = -0.030$ Å]. Also, as a result of hydrogen-bonding interactions with water, we observe an elongation of the N—H, C═O, and O—H bonds in $GlyR^{cis}$ and $GlyR^{trans}$ and the breaking of the weak intramolecular hydrogen bond (N—H1---O1═C) formed in the gas phase by $GlyR^{-}$.

The average molecular geometries of $GlyR^{cis}$, $GlyR^{trans}$, and $GlyR^{-}$ in aqueous solution are characterized by a nearly planar conformation, including the NH_2 group which has lost its pyramidal conformation observed *in vacuo*. Indeed, we have not observed any significant rotation of the NH_2 and $CO_2(H)$ groups of the glycine radical within the simulated time intervals (50 ps), but only small oscillations about the plane of the molecule. In particular, we have analyzed the probability distributions of the three dihedral angles (H1NC^{α}C, H2NC^{α}C, and N$H^{\alpha}CC^{\alpha}$) that affect the most the EPR hyperfine coupling constants. In Figure 4, such distributions are plotted for all forms of the glycine radical investigated in the present work. In all cases, an approximately symmetric Gaussian shape has been observed, with very similar distributions of the aminic hydrogen out-of-plane angles (root-mean-square amplitude, $\sigma \cong 15°$) and a sharper distribution of the N$H^{\alpha}CC^{\alpha}$ dihedral angle ($\sigma \cong 6°$). With the exception of H1NC^{α}C and H2NC^{α}C dihedral angles of $GlyR^{-}$ (see Table 4), all distributions are roughly centered at 0°, corresponding to the planar geometries. Moreover, we have analyzed the correlation among the previous dihedral angles, and we have found that, overall, between 62% and 69% of the total time, H1 and H2 are on the same side of the molecular plane, whereas H1 and H^{α} are on opposite sides (where 50% represents an uncorrelated distribution). In other words, we have observed, to some degree, a correlation of the H1NC^{α}C and H2NC^{α}C dihedral angles distributions and an anticorrelation between H1NC^{α}C and N$H^{\alpha}CC^{\alpha}$.

To proceed further, the microsolvation of $GlyR^{cis}$, $GlyR^{trans}$, and $GlyR^{-}$ has been analyzed in some detail. In Figure 5, the solvation cages of the three forms of the glycine radical are sketched by means of the spatial distribution functions (SDFs) of the surrounding water molecules, where the white and gray

Table 3. Geometrical Parameters and Dipole Moment of $GlyR^{cis}$ in Aqueous Solution Issuing from Quantum Mechanical Optimizations Using the CPCM and GLOB/ADMP Simulations

	optimized geometry (CPCM)					
	$GlyR^{cis}$					
	B3LYP[a]	B3LYP[b]	MP2[b]	$GlyR^{cis}$+4W QM/MM[c]	$GlyR^{cis}$+6W QM/MM[c]	GLOB/ADMP QM/MM[c]
N−H1	1.019	1.014	1.014	1.017	1.017	1.017
N−H2	1.017	1.012	1.012	1.020	1.020	1.016
N−C^{α}	1.349	1.346	1.343	1.347	1.345	1.353
C^{α}−H^{α}	1.087	1.081	1.080	1.087	1.087	1.086
C^{α}−C	1.424	1.420	1.421	1.421	1.419	1.426
C═O1	1.241	1.239	1.241	1.242	1.244	1.242
C−O2	1.364	1.363	1.358	1.367	1.366	1.366
O2−H3	0.990	0.986	0.990	0.983	0.980	0.984
H1−N−H2	118.32	118.47	118.98	118.11	117.78	116.7
N−C^{α}−C	120.52	120.50	119.04	121.27	121.27	120.3
O1−C−O2	121.81	121.79	122.14	120.79	121.34	121.6
H1NC^{α}C	−0.51	−0.07	−0.04	1.89	2.82	1.3
H2NC^{α}C	−179.36	−179.81	−179.87	178.68	179.21	−179.8
N$H^{\alpha}CC^{a}$	0.06	0.01	0.00	−0.40	−0.39	0.0
C^{α}CO2H3	−179.96	−179.98	−179.97	179.46	−178.61	178.2
μ	4.07	4.09	4.11	4.32	4.49	4.20

[a] N06. [b] aug-cc-pVTZ. [c] B3LYP/N06:AMBER.

Table 4. Geometrical Parameters and Dipole Moment of $GlyR^{trans}$ in the Gas Phase and in Aqueous Solution Issuing from Quantum Mechanical Optimizations and GLOB/ADMP Simulation

	gas phase		solution			
	optimized geometry		optimized geometry (CPCM)			
	$GlyR^{trans}$		$GlyR^{trans}$			
	B3LYP[a]	MP2[b]	B3LYP[a]	MP2[b]	$GlyR^{trans}$+6W QM/MM[c]	GLOB/ADMP QM/MM[c]
N−H1	1.011	1.006	1.017	1.013	1.016	1.017
N−H2	1.009	1.003	1.017	1.013	1.020	1.017
N−C^{α}	1.362	1.354	1.351	1.344	1.347	1.355
C^{α}−H^{α}	1.082	1.075	1.087	1.080	1.086	1.086
C^{α}−C	1.426	1.432	1.422	1.420	1.417	1.424
C═O2	1.224	1.216	1.242	1.241	1.247	1.244
C−O1	1.379	1.372	1.365	1.359	1.365	1.366
O1−H3	0.969	0.969	0.990	0.990	0.982	0.979
H1−N−H2	116.83	118.04	117.74	118.31	117.47	116.5
N−C^{α}−C	122.46	121.30	123.42	122.33	123.92	123.0
O1−C−O2	121.67	122.07	121.50	121.79	121.24	121.4
H1NC^{α}C	−11.38	−9.25	0.12	0.16	0.72	−0.1
H2NC^{α}C	−166.35	−169.79	−179.95	−179.97	−179.75	−179.1
N$H^{\alpha}CC^{\alpha}$	1.76	1.523	−0.01	−0.02	0.08	0.1
C^{α}CO1H3	179.65	179.75	179.97	179.99	−176.33	−179.1
μ	3.97	4.01	5.86	5.91	6.61	6.12

[a] N06. [b] aug-cc-pVTZ. [c] B3LYP/N06:AMBER.

clouds represent the water hydrogen and oxygen atoms, respectively. As expected, water molecules interact preferentially with the polar NH_2 and $CO_2(H)$ groups, whereas the aliphatic H^{α} is mainly hydrophobic. To better characterize the hydrogen-bonding pattern between the glycine radical and water, we have evaluated the average number of hydrogen bonds formed considering all the radical hydrogen atoms (H1, H2, H3, and H^{α}) as potential donors and the nitrogen and oxygen atoms (N, O1, O2) as acceptors. Results are schematically reported in Table 6. As expected, we observe in all cases a similar hydrogen-bonding pattern around the NH_2 group, whereas the number of interactions with the C-terminal group is roughly doubled on going from the neutral to the anionic form, as a result of much stronger hydrogen bonds in the latter case. The differences between Figures 3 and 5 point out that a dynamic analysis of solute vibrations and solvent librations provides an overall picture of the glycine radical in aqueous solution that is only roughly represented by a static approach based on the optimization of solute−solvent clusters embedded in a polarizable continuum.

3.3. Magnetic Properties. Before discussing our results, let us summarize the available experimental data.[7−10] The H^{α} hcc is always anomalously low (11.8 G below pH = 10 and 13.8 G above this value), the nitrogen hcc is nearly pH independent (6.4 and 6.1 G for pH values lower or larger than 10, respectively), whereas the hcc's of aminic hydrogens are strictly equivalent in acidic or neutral aqueous solutions (5.6 G), but they become slightly different at basic pH (3.4 and 2.9 G). Only isotropic values are available for the **g**-tensor, which are identical (2.00340) for neutral and anionic forms.

In order to assess our computational protocol designed to extract magnetic parameters from MD simulations (see Computational Details), the convergence of hcc's and the isotropic value of the **g**-tensor (g_{iso}) with the number of molecular

Table 5. Geometrical Parameters of GlyR$^-$ in the Gas Phase and in Aqueous Solution Issuing from Quantum Mechanical Optimizations and GLOB/ADMP Simulation

	gas phase		solution			
	optimized geometry		optimized geometry (CPCM)			
	GlyR$^-$		GlyR$^-$			
	B3LYP[a]	MP2[b]	B3LYP[a]	MP2[b]	GlyR$^-$+6W QM/MM[c]	GLOB/ADMP QM/MM[c]
N—H1	1.024	1.020	1.019	1.013	1.015	1.016
N—H2	1.016	1.010	1.018	1.013	1.019	1.015
N—C$^\alpha$	1.396	1.391	1.372	1.365	1.365	1.366
C$^\alpha$—H$^\alpha$	1.087	1.079	1.087	1.080	1.086	1.086
C$^\alpha$—C	1.486	1.485	1.457	1.454	1.448	1.448
C═O1	1.273	1.274	1.279	1.279	1.282	1.286
C═O2	1.262	1.263	1.280	1.280	1.283	1.287
H1—N—H2	112.65	113.52	115.35	116.45	116.11	115.7
N—C$^\alpha$—C	118.37	117.44	121.18	120.09	122.23	121.8
O1—C—O2	128.06	128.51	124.38	124.90	123.54	123.1
H1NC$^\alpha$C	−12.11	−13.44	−16.50	−15.71	15.82	2.6
H2NC$^\alpha$C	−138.54	−140.80	−160.56	−162.19	166.91	177.5
NH$^\alpha$CC$^\alpha$	3.14	4.26	2.66	2.70	−2.00	−0.2

[a] N06. [b] aug-cc-pVTZ. [c] B3LYP/N06:AMBER.

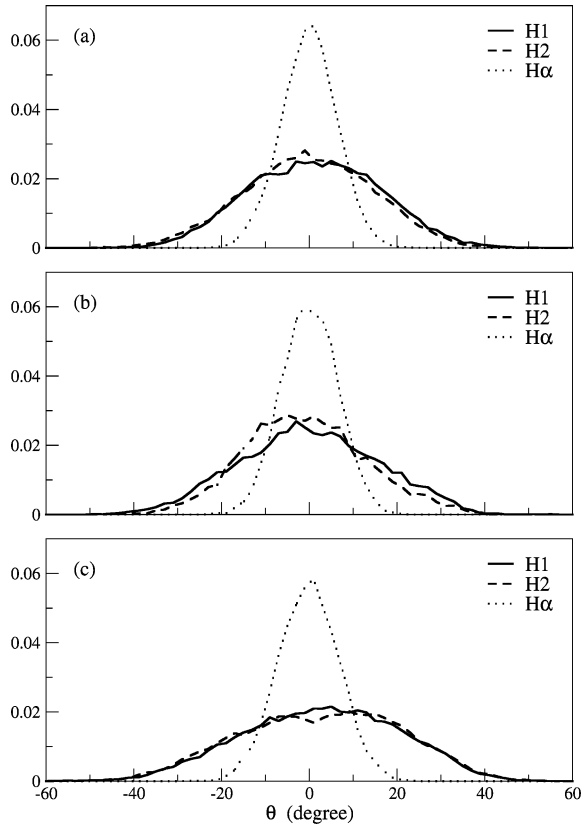

Figure 4. Probability distributions of dihedral angles (a) GlyR^{cis}, (b) GlyR^{trans}, and (c) GlyR$^-$. Note that, for convenience, the θ(H2NC$^\alpha$C) dihedral angle values have been transformed according to the formula $\theta = \sin(\theta)(180° - |\theta|)$.

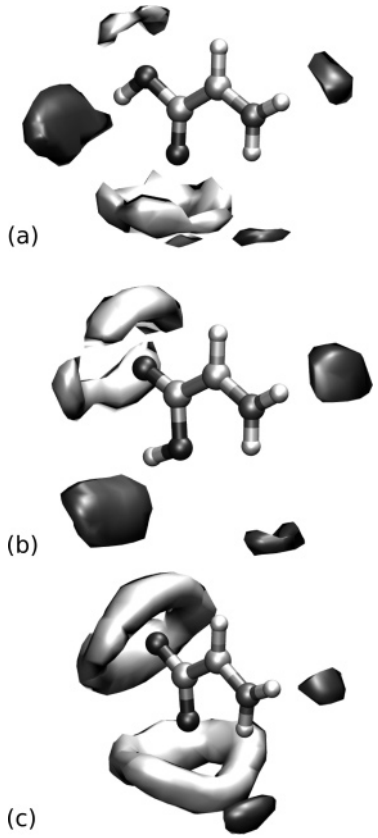

Figure 5. Spatial distribution functions of water molecules around (a) GlyR^{cis}, (b) GlyR^{trans}, and (c) GlyR$^-$ issuing from the GLOB/ADMP simulations.

configurations has been checked considering the case of Gly^{cis} in aqueous solution (see Figure 6). Similarly to what we have observed for other spectroscopic properties,[36] about 100 configurations are sufficient to reach a stable statistical average. Thus, the 500 configurations selected for computing average magnetic parameters guarantee converged results.

3.3.1. Hyperfine Couplings. In aqueous solution, both the direct solvent effect and the solvent-mediated intramolecular motions give non-negligible contributions to magnetic tensors. In an attempt to understand the interplay of such subtle effects and the importance of their relative contributions, we have evaluated the hcc's of Gly^{cis} both in the gas phase and in solution. In Figure 7, we report the absolute values of isotropic hcc's for N, C$^\alpha$, H1, H2, and H$^\alpha$ atoms, as obtained from the optimized structure of Gly^{cis} *in vacuo* and including effectively the solvent using the CPCM, and from the MD simulation by excluding or including the surrounding water molecules in the *a posteriori* calculations. On comparison of the first and second columns (or the third and fourth columns) of the histograms plotted in Figure 7, we observe that the solvent has an opposite

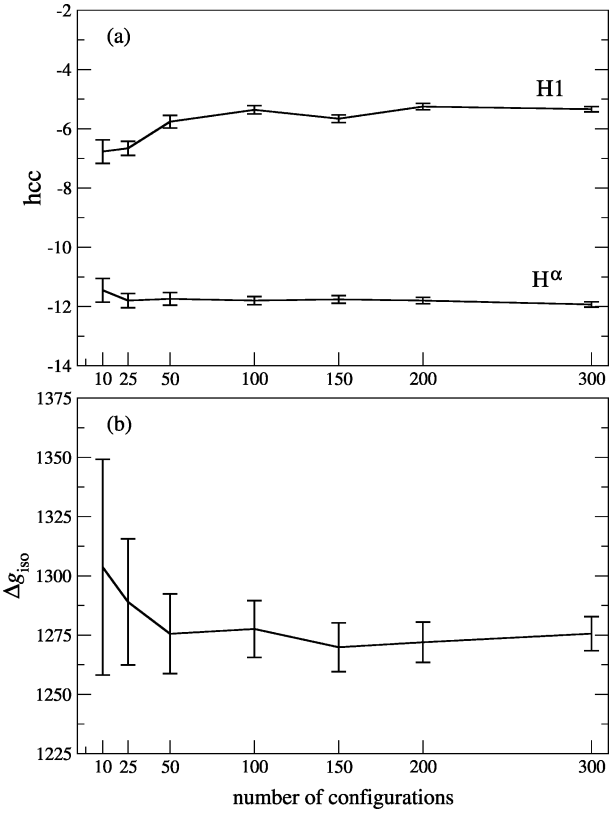

Figure 6. Convergence of the (a) hcc's of H1 and Hα and (b) Δg_{iso} (where $\Delta g_{iso} = g_{iso} - g_e$ and g_e is the g-value of the free electron, $g_e = 2.0023193$) for GlyR^{cis} in aqueous solution.

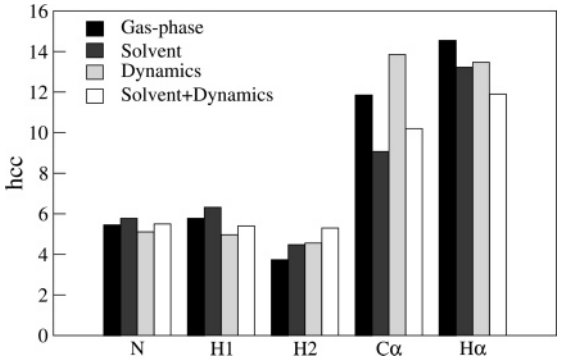

Figure 7. Hcc's of N, H1, H2, Cα, and Hα for GlyR^{cis} in the gas phase and in aqueous solutions. See text for further details. Values are in Gauss.

Table 6. Average Numbers of Solute−Solvent Hydrogen Bonds Formed by Different Atoms of GlyR^{cis}, GlyR^{trans}, and GlyR$^-$ in Aqueous Solution Issuing from the GLOB/ADMP Simulations

	GlyR^{cis}	GlyR^{trans}	GlyR$^-$
	HB Donor		
H1	0.55	0.53	0.60
H2	0.71	0.77	0.65
Hα	0.24	0.25	0.21
H3	1.00	1.00	
	HB Acceptor		
N	0.06	0.05	0.16
O1	2.08	0.50	3.63
O2	0.84	2.44	3.80

effect on the hcc's of the aminic group with respect to Cα and Hα. In the former case, the isotropic hcc's are enhanced (Δa(N) = +0.33 G, Δa(H1) = +0.55 G, Δa(H2) = +0.75 G), whereas in the latter they are lowered by more than 1 G (Δa(Cα) = −2.78 G, Δa(Hα) = −1.32 G). Moreover, dynamical effects reduce the differences between a(H1) and a(H2) on the one hand, and a(Cα) and a(Hα) on the other. It should be noted that all the QM calculations provide, as expected, positive values of the hcc's of Cα and N and negative values for the hydrogen atoms. As pointed out in previous studies,[17,18] the vibrations of the glycine radical that influence the most the spin density distribution and, consequently, the observed hcc's are the H1, H2, and Hα out-of-plane motions. As an example, we report in Figure 8 the value of a(H1) for Gly^{cis} as a function of the H1NCαC dihedral angle, freezing all the other atoms in a planar conformation previously optimized in the gas phase: in the range from 0° to 30°, a(H1) varies by more than 11 G, from a(H1) = −8.13 to 3.42 G, and the dynamical average value, corresponding to the weighted average of a(H1) on the ϕ-(H1NCαC) distribution reported in Figure 4, is −5.47 G (horizontal dotted line). Also, we have observed that a(H1) is affected, to a smaller but non-negligible extent, by the ϕ-(H2NCαC) and ϕ(NHαCCα) dihedrals. Indeed, by evaluating the weighted average effect on a(H1) of such out-of-plane modes, we have obtained an absolute shift of up to 0.3 G.

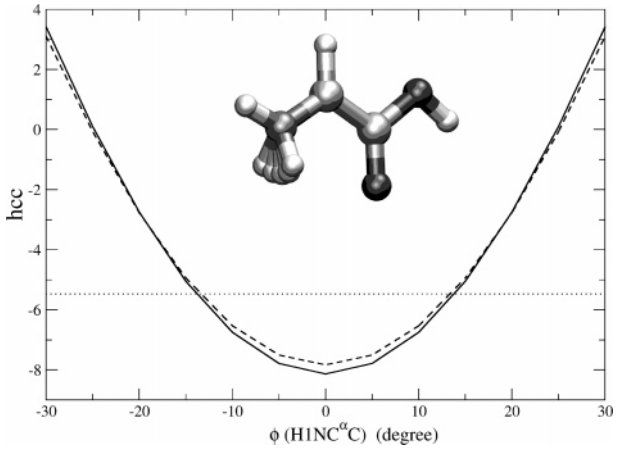

Figure 8. Hcc of H1 for GlyR^{cis} in an optimized planar structure *in vacuo* as a function of the H1NCαC dihedral angle, keeping fixed the rest of the molecule (solid line) and including the average effect of the H2NCαC dihedral angle fluctuations (dashed line). Values are in Gauss.

Furthermore, the level of agreement between theory and experiment has been checked by directly comparing the two sets of observed EPR hyperfine coupling constants of the glycine radical in aqueous solution at low and high pH[8,9] with those evaluated from the molecular dynamics simulations of the different forms of the radical considered in the present work (GlyR^{cis}, GlyR^{trans}, GlyR^{zw}, and GlyR$^-$). From Figure 9a and Table 7, we observe that the isotropic hcc's of the two neutral and non-zwitterionic forms of the glycine radical, namely GlyR^{cis} and GlyR^{trans}, are basically indistinguishable within the statistical errors (about 0.2 G) and nicely match the experimental values at low pH. On the other hand, results obtained from the GlyR^{zw} simulation deviate considerably from experiment, as expected. In the latter case, we have reported as a(H1) and a(H2) the same value, corresponding to the mean hcc of the three hydrogen bonds belonging to the amino group (NH_3^+). At basic pH, the observed hcc's are compatible with those evaluated for the anionic form of the glycine radical (see Figure 9b and Table 7). Again, we observe a very good agreement between theory and experiment. To further validate our integrated computational approach on the evaluation of EPR hcc's, at least on a qualitative

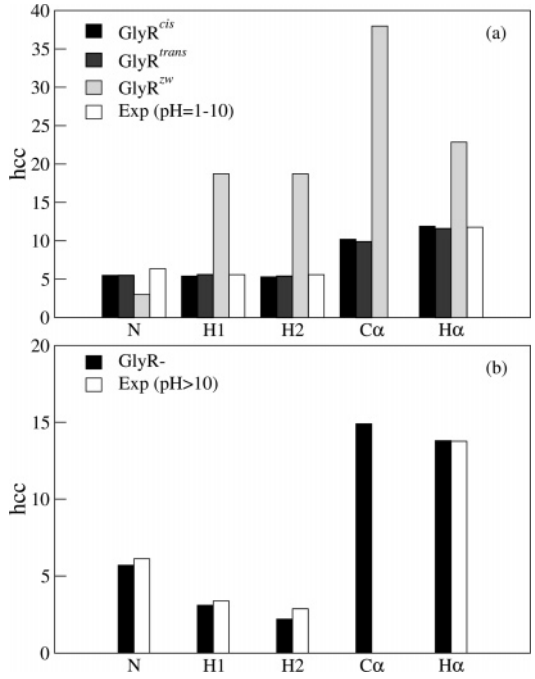

Figure 9. Comparison of the computed hcc's of (a) GlyR^{cis}, GlyR^{trans}, and GlyR^{zw}, and (b) GlyR$^-$ in aqueous solution with experimental data recorded at different pH values in ref 9. Values are in Gauss.

Table 7. Hcc's of GlyR^{cis}, GlyR^{trans}, and GlyR$^-$ in Aqueous Solution Issuing from GLOB/ADMP Simulations and Experiments (Ref 9)

	GLOB/ADMP			experimental	
	GlyR^{cis}	GlyR^{trans}	GlyR$^-$	pH = 1–10	pH > 10
a(N)	5.5	5.5	5.7	6.4	6.1
a(H1)	−5.4	−5.6	−3.1	5.6	3.4
a(H2)	−5.3	−5.4	−2.2	5.6	2.9
a(C$^\alpha$)	10.2	9.9	14.9		
a(H$^\alpha$)	−11.9	−11.7	−13.8	11.8	13.8

ground, we have considered the EPR experimental data of Sanderud and Sagstuen[12] obtained from an X-ray irradiated crystal of $NH_3^+CH_2COO^-$. From their analysis of the observed EPR signals, two forms of the glycine radical, i.e., $NH_2\dot{C}HCOOH$ and $NH_3^+\dot{C}HCOO^-$, have been assigned, and the corresponding results are reported in Figure 10, along with the hcc's for GlyR^{cis}, GlyR^{trans}, and GlyR^{zw} obtained from the MD simulations in aqueous solutions. Remarkably, even in this case, we observe a favorable agreement between theory and experiment, where the main deviations concern the hcc's of the aminic hydrogens of the zwitterionic form. However, the asymmetric arrangement of the NH_3^+ group observed in the crystals is smeared in solution, where such a group can very easily rotate as a result of the frequent breaking and forming of H-bonds.

All the above trends can be rationalized when recalling that hcc's can be decomposed in two contributions: a direct term, which is always positive, and a spin polarization contribution, which is positive at the radical center (here C$^\alpha$) and shows a characteristic sign alternation along bonding patterns moving away from it.[54] In the planar structure, the direct effect vanishes since the orbital formally containing the unpaired electron (SOMO) is a π orbital, whose nodal plane coincides with the molecular plane (see Figure 1). Spin polarization, which is

(54) Adamo, C.; Barone, V.; Subra, R. *Theor. Chem. Acc.* **2000**, *104*, 207.

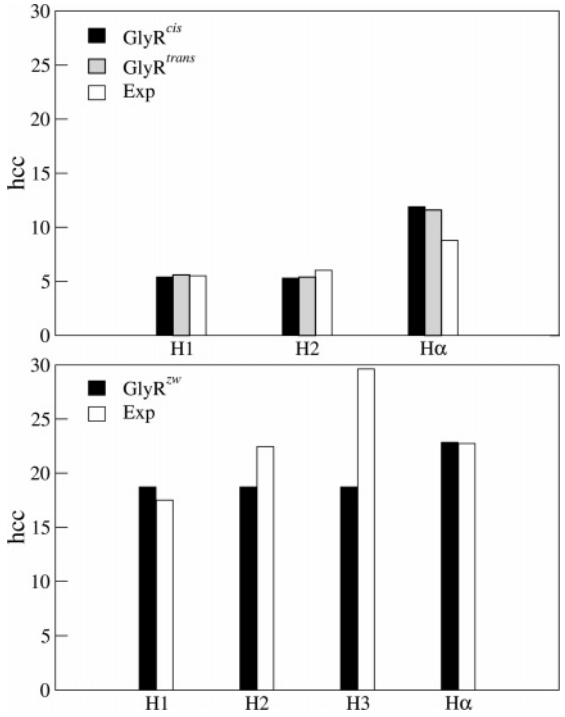

Figure 10. Comparison of the computed hcc's of (a) GlyR^{cis} and GlyR^{trans} and (b) GlyR^{zw} in aqueous solution with experimental data recorded in the solid state in ref 12.

responsible for the large negative hcc of H$^\alpha$, is proportional to the spin density at C$^\alpha$, and it is, therefore, reduced by delocalization of the SOMO. Then, the significant SOMO delocalization in GlyR$^{cis/trans}$ and GlyR$^-$ explains the anomalously small value of the H$^\alpha$ hcc, which increases significantly in GlyR^{zw}, due to the reduced delocalization of the SOMO (see Figure 1). Solvent effects do enhance the delocalization along the backbone, due to an increased weight of ionic resonance structures involving double N−C$^\alpha$ or C$^\alpha$−C′ bonds with the consequent reduction of the H$^\alpha$ hcc and of the pyramidality of the aminic moiety. Spin polarization effects are nearly constant for H1 and H2, so that their hcc's are modified essentially by the direct effect (i.e., direct contribution to the SOMO), which is, of course, enhanced by displacement above or below the average molecular plane. Since solvent effects lead from a strongly pyramidal to a nearly planar species, they involve a dramatic reduction of the H2 hcc and an increased delocalization of the SOMO with the consequent reduction of the π spin density on C$^\alpha$ and of the H$^\alpha$ hcc.

3.3.2. g-Tensors. Let us now consider in some detail the **g**-tensor of glycine radical. The radical center being located on the C$^\alpha$ atom, which scarcely interacts with the environment, experiments detect a quite small anisotropy of the *g*-values compared to other amino acid radicals. Moreover, in aqueous solution, only the isotropic *g*-value has been measured, which is equal to 2.00340 ± 0.00005 for both acidic and basic pH values.[9] In Figure 11, the *g*-values and the corresponding principal axis system for GlyR^{cis}, GlyR^{trans}, and GlyR$^-$ are reported, as computed in the gas phase. As pointed out in previous studies,[21,22] **g**-tensors are more sensitive to the conformation of the radical than hyperfine tensors; e.g., the **g**-tensors of GlyR^{cis} and GlyR^{trans} are significantly different. In particular, we have analyzed the influence of individual geometrical changes, such as bond stretching and bending. The

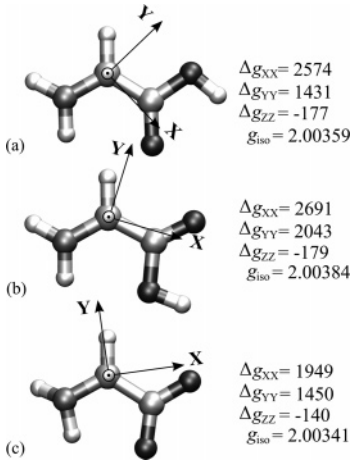

Figure 11. **g**-tensor principal axes and values (shifts with respect to g_e in ppm) and g_{iso} for (a) GlyR^{cis}, (b) GlyR^{trans}, and (c) GlyR$^-$ in the gas phase. The *Z*-axis is perpendicular to the molecular plane.

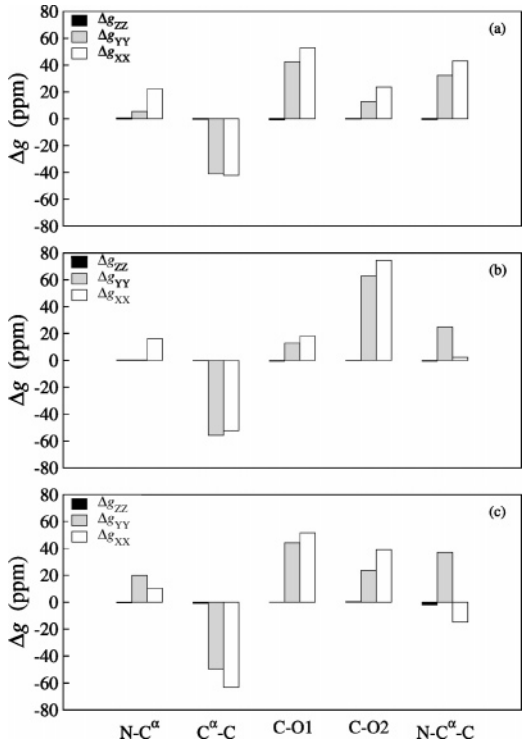

Figure 12. **g**-tensor values for (a) GlyR^{cis}, (b) GlyR^{trans}, and (c) GlyR$^-$ in the gas phase as a function of individual geometrical parameters. Bond lengths are incremented by 0.01 Å and the N−C$^\alpha$−C bond angle by 2°.

results reported in Figure 12 show that the Δg_{XX} and Δg_{YY} components (where $\Delta g_{\alpha\alpha}$ stays for $g_{\alpha\alpha} - g_e$ and g_e is the *g*-value of the free electron, $g_e = 2.0023193$) experience significant changes upon modification of the C$^\alpha$—C and C═O (double) bonds and, to a lower extent, upon modification of the N—C$^\alpha$ and C—O (single) bonds and the N—C$^\alpha$—C angle. On the other hand, out-of-plane motions do not alter appreciably the **g**-tensor, except for a slight effect on the component normal to the average molecular plane (Δg_{ZZ}). It is worth noting that such results are consistent with the fact that the largest contribution to the **g**-tensor of the glycine radical is provided by the spin−orbit coupling term, which involves mainly the lone pairs on the oxygen atoms. Moreover, we have observed an overall good agreement between **g**-tensors computed on optimized geometrical structures obtained at DFT B3LYP level and post-Hartree−Fock (MP2 and CCSD(T)) methods, with deviations that tend to decrease by including solvent effects (see, e.g., the comparison between B3LYP and MP2 using the CPCM, as shown in Table 8).

Table 8. **g**-Tensor Values (Shifts with Respect to g_e) and g_{iso} for GlyR^{cis}, GlyR^{trans}, and GlyR$^-$ in Aqueous Solution Issuing from Quantum Mechanical Optimizations Using the CPCM and GLOB/ADMP Simulations and Experiments (Ref 9)

	optimized geometry			
	B3LYP	MP2	GLOB/ADMP	expt
		GlyR^{cis}		
Δg_{XX}	2657.0	2607.5		
Δg_{YY}	1458.4	1433.3		
Δg_{ZZ}	−191.4	−190.9		
g_{iso}	2.00363	2.00360	2.00359	2.00340
		GlyR^{trans}		
Δg_{XX}	2636.3	2612.4		
Δg_{YY}	1976.3	1925.3		
Δg_{ZZ}	−190.4	−189.9		
g_{iso}	2.00379	2.00377	2.00375	2.00340
		GlyR$^-$		
Δg_{XX}	2172.8	2161.4		
Δg_{YY}	1728.2	1712.2		
Δg_{ZZ}	−182.2	−182.1		
g_{iso}	2.00356	2.00355	2.00356	2.00340

In analogy with the previous analysis on the hcc's, we have considered separately the direct and indirect effects of the solvent on the magnetic response of the glycine radical. From Tables 2−4 (geometrical parameters) and Figure 12, it is apparent that, considering only the geometrical changes of the glycine radical induced by the solvent, the **g**-tensors are generally enhanced, especially the Δg_{XX} and Δg_{YY} terms. Specifically, we have evaluated the increase of g_{iso} from the gas phase (optimized structures, Figure 11) to the aqueous solution (MD simulations, excluding the direct solvent effects of the water molecules and retaining only the geometrical and dynamical effects). As expected, we have obtained a larger increase for GlyR$^-$ ($\Delta g_{iso} \cong +340$ ppm) with respect to GlyR^{cis} ($\Delta g_{iso} \cong +90$ ppm) and GlyR^{trans} ($\Delta g_{iso} \cong +110$ ppm). On the contrary, the solvent polarization effects, especially via the formation of hydrogen bonds with the oxygen atoms of the glycine radical, do induce a reduction of the *g*-factors. Therefore, the overall change of the *g*-values is quite small in all cases considered (see results reported in Figure 11 (gas phase) and Table 8 (aqueous solution)).

Finally, we have compared the results obtained from the MD simulations of GlyR^{cis}, GlyR^{trans}, and GlyR$^-$ with the only available experimental data, i.e., g_{iso}. As reported in Table 8, our results are somewhat higher than their experimental counterparts, even considering the statistical noise (about 50−60 ppm). Interestingly, GlyR^{cis} and GlyR$^-$ show very similar g_{iso} values (2.00359 and 2.00356, respectively), whereas the g_{iso} of GlyR^{trans} is appreciably larger (2.00375). Such results could suggest, assuming a systematic error of the computational methodology employed,[21,22] that the favored conformation of the glycine radical in aqueous solution is the cis form at pH < 10. Indeed, quantum mechanical calculations on GlyR^{cis} and GlyR^{trans} using the CPCM or with small water clusters have shown that the cis form is more stable by about 0.5 kcal/mol (0.49 kcal/mol for clusters with six water molecules + CPCM and considering the solute at CCSD(T) level; 0.36 kcal/mol for clusters with six water molecules + CPCM at the B3LYP level).

4. Conclusions

In the present paper, we have reported the essential results of a comprehensive analysis of the structure, dynamics, and EPR parameters of the radicals derived from homolytic breaking of the $C^{\alpha}-H^{\alpha}$ bond of glycine in aqueous solution at different pH values. We have unraveled the role of intrinsic structural preferences, solvation patterns, and short-time dynamical effects in determining the experimental EPR spectrum. In particular, solvent effects play a significant role for the neutral form and completely modify the EPR spectrum for the anionic form. At the same time, out-of-plane motions of the NH_2 and $C^{\alpha}H^{\alpha}$ moieties, although they are only weakly coupled, have a synergic effect in averaging proton hyperfine couplings. Thus, our study offers a rich and internally consistent picture of magneto-structural relationships and of dynamical features for a prototypical amino acid in aqueous solution, bridging in a consistent and direct way macroscopic observables and detailed microscopic dynamics of a quite complex system.

From a more general point of view, the results of the present study confirm that hybrid functionals coupled to purposely tailored basis sets allow researchers to compute magnetic tensors in remarkable agreement with their experimental counterparts: computed data can take into the proper account both environmental effects and short-time dynamical contributions like, e.g., vibrational averaging from intramolecular vibrations and/or solvent librations, therefore providing a set of tailored parameters that can be confidently used for further calculations. The ongoing integration[25] of improved QM methods for the calculation of magnetic tensors, and effective implementations of approaches based on the stochastic Liouville equation for increasing numbers of degrees of freedom, further widens the range of application of computational approaches,[26] paving the route toward full *a priori* simulations of EPR spectra in different phases and over large temperature intervals.

Acknowledgment. The authors thank the Italian Research Ministry for University and Research (MIUR) and Gaussian Inc. for financial support. All computations were performed on the large-scale computer facilities of the VILLAGE network (http://village.unina.it).

Supporting Information Available: Complete ref 53. This material is available free of charge via the Internet at http://pubs.acs.org.

JA074910T